Acta Materialia 203 (2021) 116461

Contents lists available at ScienceDirect

Acta Materialia

journal homepage: www.elsevier.com/locate/actamat

Substrate stoichiometry changes during pulsed laser deposition: a case study on $SrTiO_3$

Matthäus Siebenhofer[a,*], Tobias Huber[a,c], Werner Artner[b], Jürgen Fleig[a], Markus Kubicek[a]

[a] Institute of Chemical Technologies and Analytics, TU Wien, Austria
[b] X-Ray Centerwwww, TU Wienw, Austria
[c] Kyushu University, Next-Generation Fuel Cell Research Center (NEXT-FC)wwww, Japan

ARTICLE INFO

Article history:
Received 24 June 2020
Revised 28 September 2020
Accepted 31 October 2020
Available online 10 November 2020

ABSTRACT

The influence of UV illumination by the plasma plume on the substrate stoichiometry during pulsed laser deposition (PLD) was examined on the model perovskite $SrTiO_3$ (STO) by the means of *in situ* impedance spectroscopy during pulsed laser deposition (IPLD). In this manner, the evolution of the STO bulk conductivity was tracked at 300 °C during STO thin film deposition and during deposition on a quartz cover to isolate illumination effects from deposition effects. These measurements revealed an increasing bulk conductivity during covered measurements. Impedance spectroscopy under applied bias voltages indicates that these changes are not caused by photovoltages but by an enhanced oxygen incorporation compensated by electron hole generation under UV illumination. This enhanced conductivity persists after illumination. The combination of across-plane and in-plane measurements further indicates the formation of a layered system, allowing to estimate conductivity and thickness of the newly formed oxygen vacancy deficient layer. This results in a ~30 times more conductive top layer with a thickness of ~40 μm. The driving force induced by the UV illumination which is responsible for this stoichiometry change corresponds to a $p(O_2)$ difference of around six orders of magnitude. Results of in situ measurements show that the real deposition of a thin film leads to a more complex layered system where the growing film interacts with the illuminated top layer of the substrate and possibly introduces additional oxygen vacancies. These changes have a strong influence on any grown thin film either by oxidation/reduction potential or lattice parameter changes.

1. Introduction

Pulsed Laser Deposition (PLD) is a well established and highly versatile physical deposition method, suitable for a diverse range of materials and widely used in various fields of research, mainly for the growth of complex oxide films [1–3]. Although the concept of PLD is simple, the underlying processes and their interactions are comparatively complex and all have a substantial influence on the final film properties [4]. Whereas the influence of substrate temperature, laser fluence and target distance as well as pressure of the ambient carrier gas on the properties of thin films deposited with PLD is frequently investigated [5–9], the interaction of the substrate with the PLD plasma plume is rarely studied. Only recently it was shown that at high temperatures and low oxygen partial pressures the oxygen excorporation rate of $SrTiO_3$ is significantly increased under UV illumination in the PLD [10]. Similar effects were discovered when thin films were deposited on $SrTiO_3$ and oxygen deficient regions in the substrate due to reducing effects during PLD deposition were observed [11–13]. In contrast to these studies, it was also shown that the oxygen incorporation rate of STO is significantly increased during conventional UV illumination at high temperatures [14], which manifests in the form of photovoltages, enhanced conductivity and high temperature photochromism [15–17]. It is because of these complex processes and diverse experimental results, that the effect of the plasma illuminating the substrate has become increasingly intriguing, since the condition of the substrate can influence thin film properties significantly with regard to stoichiometry, structure and morphology.

In this article, the impact of the deposition process on the electrical and defect chemical properties of the model substrate $SrTiO_3$ (STO) was investigated with In Situ Impedance Spectroscopy during Pulsed Laser Deposition (IPLD) [18,19]. This technique allows to probe electrochemical properties of the substrate directly dur-

* Corresponding author. E-mail address: matthaeus.siebenhofer@tuwien.ac.at

https://doi.org/10.1016/j.actamat.2020.10.077

ing the PLD process. The effects of UV radiation from the plasma were isolated from potentially disrupting effects from impinging species, which allows the analysis of the basic interaction between the UV light from the plasma plume and the substrate. The results of these measurements show that under UV illumination in the PLD, the oxygen incorporation rate is increased, and an oxygen enriched and more (electron hole) conductive layer develops in the substrate. These results are also compared with the effects during deposition and support the assumption that the growing thin film reduces the substrate underneath.

2. Methods

2.1. Sample preparation

Current collector grids (100 nm Pt, 35 μm square holes / 15 μm stripes) were prepared by lift-off photolithography and metal sputtering (Bal Tec MED 020, Leica Microsystems GmbH, Germany) on one side of (100) oriented $SrTiO_3$ (STO, Crystec GmbH, Germany) single crystalline substrates (5 x 5 x 0.5 mm^3). This grid ensured that across-plane conductivity measurements were possible and that UV radiation could still penetrate the 49% grid-free surface (see S.1). The exact free area was calculated from optical microscope images after platinum deposition. The back side was completely covered with sputtered platinum to provide optimal contact surface. For in-plane measurements two opposite side faces of a (100) oriented $SrTiO_3$ (STO, Crystec GmbH, Germany) single crystalline substrates (10 x 10 x 0.5 mm^3) were covered with platinum paste (Tanaka Europe GmbH) and a very small spot (diameter ~0.5 mm) was painted on the top adjacent to the sides as a contact point for the needles.

2.2. In-situ Impedance Spectroscopy during PLD (IPLD)

For the experiments conducted in this work a new PLD sample holder was designed and constructed (Huber Scientific, Austria), allowing for simultaneous heating of the sample and the performance of electrochemical measurements during deposition processes. A sketch of the heater stage is shown in chapter S.2 of the supporting information. The heater itself is built from an Al_2O_3 block with embedded platinum meanders used for resistive heating. Also embedded into the heater is a type S thermocouple to measure the temperature. The sample temperature was linked to the heater temperature via calibration with a YSZ single crystal prepared similarly to the STO samples used in the remaining experiments. The high frequency minimum or real axis intercept occurring in impedance spectra of YSZ single crystals is caused by the ionic conduction of YSZ and by the internal resistance of the setup. In combination with the known temperature-conductivity relation of YSZ single crystals, the sample temperature can be determined reliably [19,20]. A direct calibration with the resistivity of STO was not viable due to the observed stoichiometry changes and long equilibration times. The heater stage further offers the possibility to contact a sample with up to four platinum needles, as well as with a plane platinum electrode painted directly on the Al_2O_3 block. Furthermore, a quartz plate can be mounted on the heater to cover the sample and prevent actual deposition while allowing UV radiation to reach the sample.

The transmission of the quartz plate for radiation with a wavelength between 250 and 400 nm was measured to be ~75% with an UV-vis absorption measurement setup (tungsten lamp by Edmund Optics Inc., Germany and Ocean Optics QE6500 spectrometer by Halma plc, England). The quartz plate was continuously repolished after the deposition of 2000 pulses to minimize the absorption of UV radiation by layers deposited on top of the quartz plate. A more detailed analysis of the power density and the wavelengths of the UV light reaching the sample is shown in S.2, as well as photographs of the setup in operation.

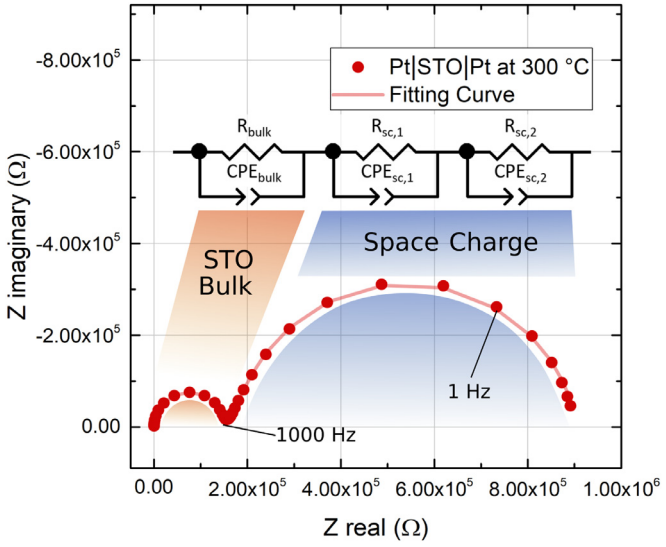

Fig. 1. Impedance spectrum of an STO single crystal with platinum grid on top and a sputtered platinum electrode on the bottom side at 300 °C and 0.06 mbar $p(O_2)$. All impedance data were fitted using the equivalent circuit in the figure.

For all IPLD measurements a polycrystalline $SrTiO_3$ target was used. It was placed either 6 cm above the quartz cover (and 9 cm above the sample) or 6 cm above the sample depending on whether material was deposited on the sample or not. The atmosphere during measurements was always set to 0.06 mbar $p(O_2)$ and the sample was heated to the desired temperature. A KrF ($\lambda = 248$ nm) excimer laser (Lambda Physics, COMPex Pro 201) with a laser fluence of 2 J/cm^2 was used for all depositions with a frequency of 1 Hz.

All impedance measurements were conducted with an Alpha-A High Performance Frequency Analyzer and Electrochemical Test Station POT/GAL 30V/2A setup by Novocontrol Technologies in a frequency regime from 10^6 to 10^{-2} Hz. Measurements were performed with a resolution of 5 points per decade and an AC_{RMS} voltage of 20 mV.

3. Results and Discussion

3.1. In Situ Impedance Spectroscopy on $SrTiO_3$ single crystals

Across-plane impedance spectroscopy inside the PLD chamber was the main experimental method used in this work. For such measurements the sample temperature was usually kept at 300 °C and the atmosphere was set to 0.06 mbar $p(O_2)$. A typical impedance spectrum achieved in these experiments is shown in Fig. 1 together with the equivalent circuit used to fit the data.

In all impedance spectra two features were clearly visible. In the high frequency regime a nearly ideal semicircle was observed. The impedance of this semicircle was quantified with an equivalent circuit fit of the spectrum to a R-CPE element (CPE = constant phase element). From the fitted parameters of the CPE element, the capacitance of the real physical object can be calculated with the relations [21]

$$Z_{CPE} = Q^{-1}(i\omega)^{-n} \text{ and } C = (R^{1-n} \cdot Q)^{1/n}, \quad (1)$$

using the fit parameters Q and n. With this calculation the first semicircle typically yields capacitance values of $6.7 \cdot 10^{-11}$ F. Together with the geometry of the sample this corresponds to a permittivity of $\epsilon = 150$ which is in good agreement with values for

STO single crystals at comparable temperatures found in literature [22–24]. Thus, the first semicircle is attributed to the bulk of the STO single crystal. The bulk resistance, R_{bulk}, for equilibrated samples at 300 °C and 0.06 mbar was in the range of 160 kΩ for all samples, which results in a total conductivity of $1.25{\cdot}10^{-6}$ S/cm. Further details on the equilibration process are presented in S.5.

The second impedance feature is a less ideal semicircle and can be fitted very well with two R-CPE elements. This yields one predominant element with a capacitance of around $1.5{\cdot}10^{-7}$ F which constitutes around 90% of the resistance of the whole feature, R_{sc}. The second feature is significantly smaller and its capacitance is in the same order of magnitude. We suspect that these features can be ascribed to the space charge at the interface between the platinum current collector and the $SrTiO_3$ single crystal. Taking account of the reduced contact area at the top side with the current collector grid, we get an interfacial capacitance of around $2.1{\cdot}10^{-6}$ F/cm^2 for the dominant feature. For a first approximation of the space charge layer thickness, a simple parallel plate geometry is assumed:

$$C = \epsilon\epsilon_0 \frac{A}{d}. \tag{2}$$

For the above calculated interfacial capacitance and the bulk permittivity determined above, this results in a space charge zone of 63 nm. If the space charge follows the behaviour of an electronic Schottky barrier, this thickness can be correlated with the charge carrier concentration. The thickness of a Schottky barrier can be estimated with [25]

$$x_d = \sqrt{\frac{2\epsilon\epsilon_0|\Delta\phi|}{qN_d}}, \tag{3}$$

where $\Delta\phi$ is the potential difference at the interface between electrode and bulk material, q is the elemental charge and N_d is the dopant concentration. This potential difference is typically a few 100 mV, assuming ϕ_{Pt}=5.64 eV for the work function of platinum [26] and ϕ_{STO}=5.85 eV for the Fermi level of STO [27] (both values for room temperature), we end up with $|\Delta\phi|$=210 mV. When compared with the thickness calculated above, this yields a charge carrier concentration of 26 ppm which is a reasonable value for impurity dopants in nominally undoped STO, which is known to be in the range of tens of ppms [28,29]. The exact situation may be complicated by additional ionic charge carriers but values most probably remain in the same order of magnitude. Thus we can confidently assign the second impedance feature to the space charges at the Pt/STO interfaces.

When impedance measurements were continued to frequencies below 1 Hz, a third feature appeared at the low frequency end of the impedance spectrum. We suspect that this feature describes the change from mixed ionic electronic to purely electronic conductivity. As examination of this feature requires significantly longer measurement times, this arc was not measured during the experiments presented in this work.

For in-plane impedance measurements, the same two fundamental impedance features appear but both on a different resistance scale, which is expected due to the geometry change (Fig. 2). Changes of the space charge feature are also expected because of the brushed Pt contacts which introduce a potentially very different $|\Delta\phi|$, compared to sputtered Pt electrodes (due to different orientations and possibly different interfacial states). Furthermore, the first feature is slightly distorted inwards at the end of the semicircle. Such distortions are known to occur in our measurement geometry (in-plane with the heater acting as a parasitic capacitance) and are mentioned in literature [30]. For a very detailed analysis a sophisticated equivalent circuit was suggested [31]. With this equivalent circuit the impedance spectra could be fitted very well as shown in Fig. 2. During pulsing, only the first feature of the

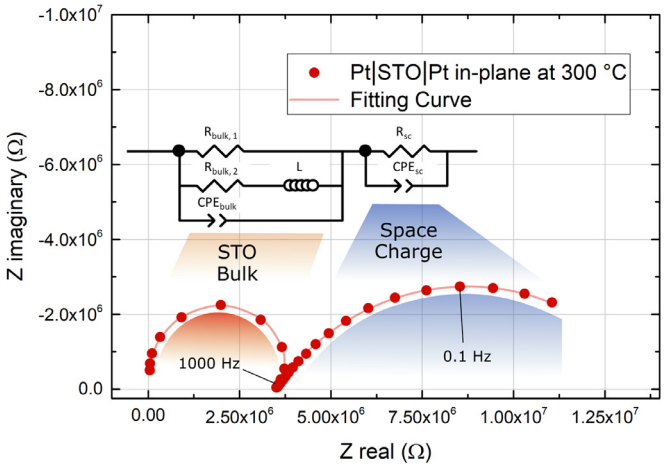

Fig. 2. In-plane impedance spectrum of an STO single crystal with two platinum coated side faces at 300 °C and 0.06 mbar p(O_2) after 1000 laser pulses on a quartz cover. All impedance data were fitted using the equivalent circuits in the figure [31].

spectrum was recorded to reduce the measurement time and avoid relaxation processes, as a proper investigation of the space charge feature would require measurement frequencies below 100 mHz.

These measurements revealed slightly different values for material properties. While the bulk conductivity after equilibration before any laser pulses was measured to be $1.5{\cdot}10^{-6}$ S/cm, which is very close to across-plane measurements, the relative permittivity of the bulk STO was slightly lower (ϵ=110). The capacitance of the space charge was slightly higher ($7.84{\cdot}10^{-6}$ F/cm^2) than during across-plane measurements.

3.2. UV irradiation of quartz covered $SrTiO_3$ by the PLD plasma plume

Impedance measurements on STO substrates were performed across-plane and in-plane during PLD deposition on a quartz plate mounted above the sample. Measurements were performed after 1, 3, 10, 30, 100, 300 and 1000 pulses. To assess the total illumination time, the PLD process was filmed with a Sony DSC RX10 MIII camera in high-speed mode with a frame rate of 1000 fps. These recordings revealed that the time when the plasma plume is optically visible is lower than 1 ms. Highly time resolved photography and measurements from other authors show that the duration of the plasma plume is actually significantly lower, being rather in the range of tens of microseconds [32–34]. For 1000 pulses the total illumination time in our measurements is therefore less than 0.1 s. The results of these measurements are shown in Fig. 3.

During across-plane measurements a reduction of the bulk resistance by 7% was observed after 1000 pulses, while the space charge feature at first remains unaffected and then shows a slight resistance increase after 30 pulses. The capacitive properties of both features are unaffected by the illumination. Importantly, in-plane measurements during illumination reveal an even stronger decrease of the bulk resistance by over 70% after 1000 pulses. Both, across- and in-plane changes remain after the experiment. Post-illumination phenomena are discussed later on.

From experimental data the large difference between in-plane and across-plane measurements strongly indicates a layered system with regions of different conductivities. Employing a simple model with a well defined top layer of spatially constant but enhanced conductivity (σ_{UV}), the combination of across-plane (a.p.) experiments (with the total resistance dropping by 7%) and in-plane (i.p.) experiments (with the total resistance dropping by 70%), while neglecting the potential temperature difference and as-

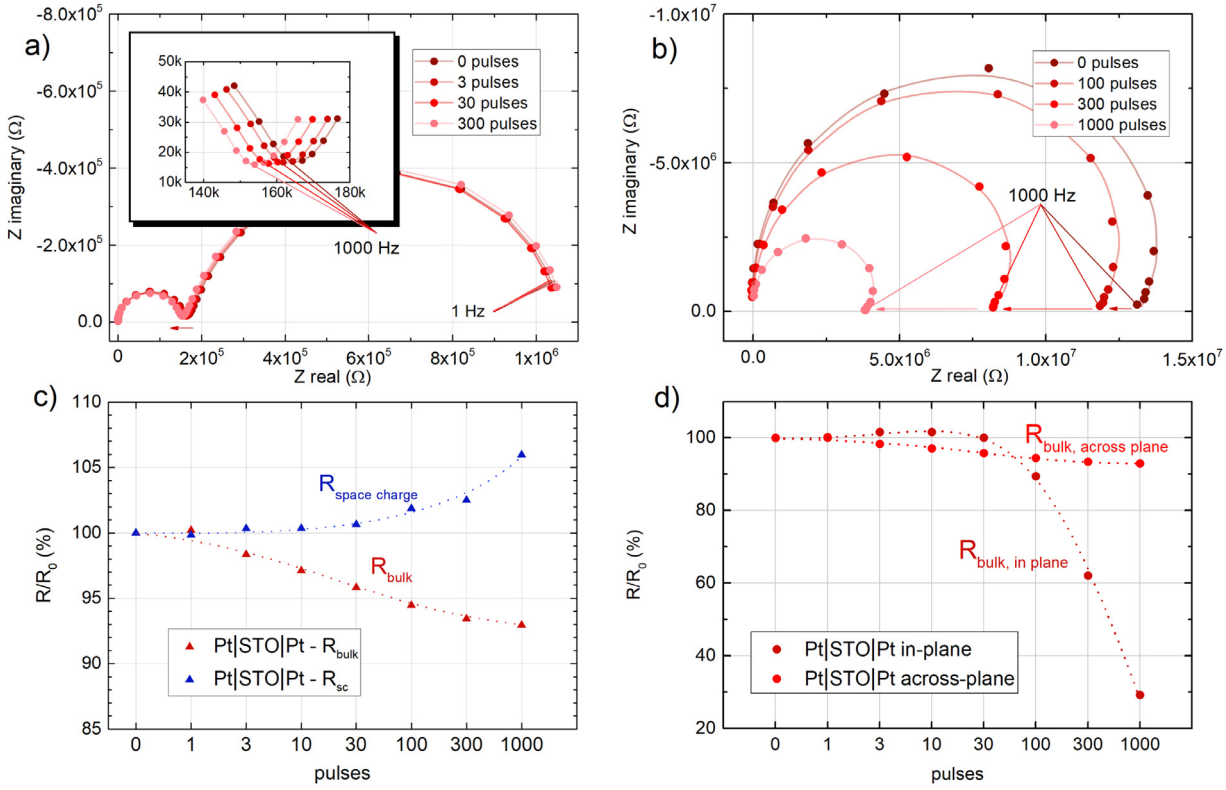

Fig. 3. Impedance spectra measured at 300 °C during laser pulses on a quartz covered sample measured across-plane (a) and in-plane (b), for in-plane measurements only the bulk part was measured. The evolution of resistances relative to their starting value R_0 is shown in c) for across plane measurements and in d) for in-plane measurements compared to across-plane measurements. Dotted lines in c) and d) are a guide for the eye.

suming the same initial conductivity, also allows an estimate of the thickness and the conductivity of this new layer using electrochemical measurement results via the following relations:

$$\begin{aligned} &l \text{ across-plane}: R_{tot,a.p.} = R_{1,a.p.} + R_{2,a.p.} \longrightarrow \frac{0.93 \cdot d}{\sigma_0} = \frac{x}{\sigma_{UV}} + \frac{d-x}{\sigma_0}, \\ &l \text{ in-plane}: \frac{1}{R_{tot,i.p.}} = \frac{1}{R_{1,i.p.}} + \frac{1}{R_{2,i.p.}} \longrightarrow \frac{\sigma_0 \cdot d}{0.30} = \sigma_{UV} \cdot x + \sigma_0 \cdot (d-x), \end{aligned} \tag{4}$$

where 1 and 2 represent the two different layers, d is the sample thickness, x the thickness of the highly conductive layer and σ_0 is the original conductivity of the sample. A sketch of this situation is shown in Fig. 4.

Solving these equations results in a 33 times more conductive top layer with a thickness of 36 μm. Classical photoconductivity, which has been frequently examined in $SrTiO_3$ [35–37], cannot explain the observed effects, on the one hand due to the small absorption depth of about 1 μm and on the other hand because the effect is persistent after the experiment despite a measurement temperature of 300 °C (see below). The most probable origin of such different conductivities lies in a different defect chemistry of the two layers. Throughout the last decades two fundamental processes were shown to cause stoichiometry changes in STO - electrocoloration by applying DC voltages and enhanced oxygen incorporation under ultraviolet illumination [14,16,38–40]. In the following we will try to identify the process responsible for the effects observed in our experiments.

It is well known from earlier studies that during illumination, a photovoltage is induced at the platinum-STO interface [15]. To test, if a photovoltaic effect is the reason for the stoichiometry change and the observed increase in conductivity, bias voltage was applied in the in-situ setup at a temperature of 330 °C. The results of these measurements are shown in Fig. 5 (for more data on the voltage response of $SrTiO_3$ to the plasma plume, see S.6). Application of

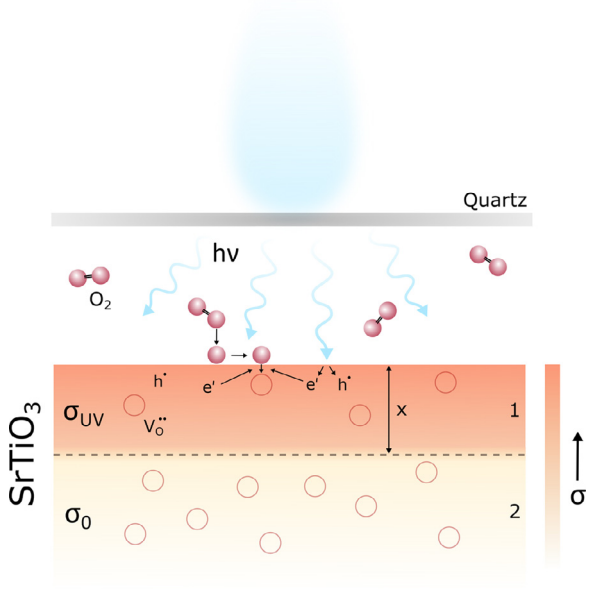

Fig. 4. Sketch of the resulting layer structure of the sample including a schematic of the accelerated oxygen incorporation process under UV illumination during PLD.

100 mV bias voltage indeed resulted in a slight change of the bulk resistance, for 100 mV positive bias voltage, the effect is similar as during illumination. However, while the space charge resistance was nearly unaffected during PLD pulses, it changed significantly during the application of bias voltage. Therefore, we conclude that the photovoltage does not cause the observed changes in our IPLD

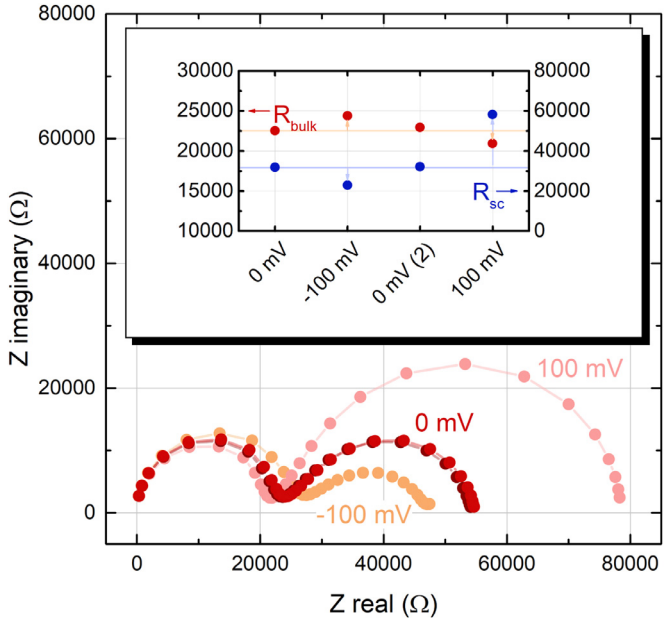

Fig. 5. Impedance spectra and resistance values during the application of different bias voltages from -100 mV to 100 mV at 330 °C.

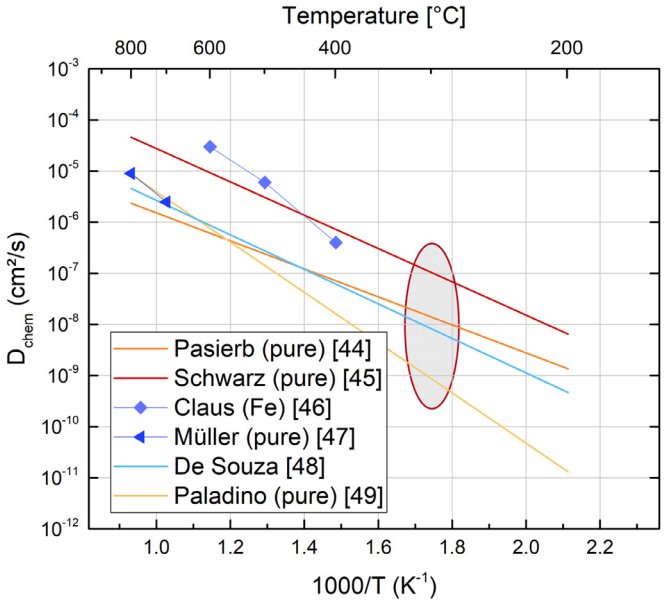

Fig. 6. Chemical diffusion coefficients of undoped (pure) and Fe-doped $SrTiO_3$ in a wide temperature range from 200 to 900 °C. Symbols represent actual measurement values, lines without measurement values show the analytic expressions given by the corresponding authors. The highlighted area marks relevant diffusion coefficients for the present work.

measurements and that no electrical degradation takes place in our experiments.

With regard to our second assumption, several indications can be found in literature that UV illumination has a significant influence on the surface oxygen exchange of STO single crystals [10,14,15] At elevated temperatures, the STO surface is in equilibrium with the surrounding gas phase, governed by the oxygen exchange reaction

$$\frac{1}{2}O_2(gas) + V_O^{\cdot\cdot} \rightleftharpoons O_O^x + 2h^{\cdot}, \tag{5}$$

which is comprised of a number of steps, from adsorption to ionization and incorporation [41–44]. As shown in [15], under continuous UV illumination at similar temperatures to the experiments presented in this work, the equilibrium of this oxygen exchange reaction shifts towards the incorporation reaction, most probably caused by the increased concentration of conduction band electrons under UV illumination. We therefore assume that also during pulsed laser deposition, the oxygen incorporation is accelerated and leads to a change in the stoichiometry of the near-surface region. Oxygen vacancies are annihilated and the electron hole concentration is increased. The latter causes the conductivity increase in the top layer (σ_{UV}). Since this is a true defect chemical change rather than photoconductivity, the enhanced conductivity also persists after the illumination (see below).

According to diffusion theory this strong stoichiometry imbalance at the surface should equilibrate into the single crystal. Literature research yields a variety of possible chemical diffusion coefficients for doped and undoped $SrTiO_3$, a selection is shown in Fig. 6, ranging over two orders of magnitude from 10^{-9} to 10^{-7} cm^2/s [45–50]

With a total experiment time of around 1800 s at the time of the measurement after 1000 pulses, the average diffusion distance of $\langle x \rangle = 2\sqrt{\frac{Dt}{\pi}}$ ranges between 15 and 150 μm [51], the calculated layer thickness of 36 μm being in good agreement with this range and corresponding to a chemical diffusion coefficient of $6{\cdot}10^{-9}$ cm^2/s. We therefore hypothesize that UV illumination in the PLD leads to a layered system with different oxygen non-stoichiometries. A more conductive and oxygen rich layer is formed in the upper part of the sample, while the rest remains relatively unaffected and therefore shows a higher oxygen vacancy concentration (see Fig. 4).

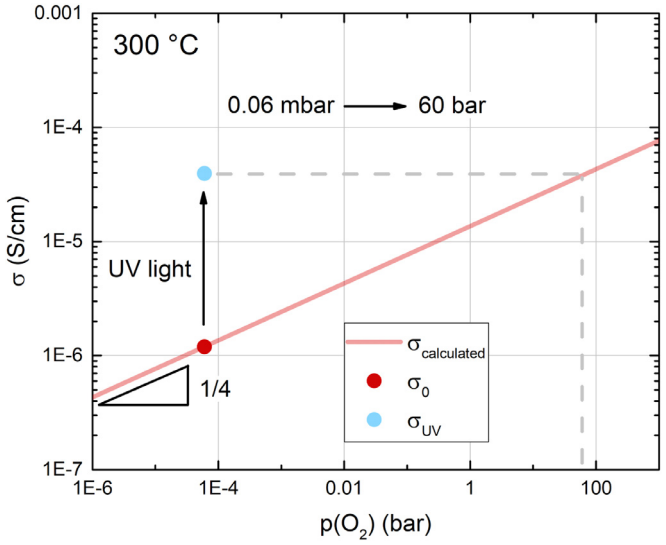

Fig. 7. Calculated (hole) conductivity at 300 °C for $SrTiO_3$ compared to measurement results before and after UV illumination in the PLD.

For a better understanding of what driving force is generated by the illumination, these results are visualized in a conductivity-p(O_2) diagram (see Fig. 7) for an initial conductivity of $1.2{\cdot}10^{-6}$ S/cm. Under the given conditions hole conductivity dominates the total conductivity σ_0. The hole conductivity values for STO at 300 °C were calculated according to the model developed by Denk et al. [52] with an impurity content of 26 ppm (from space charge analysis). The model was slightly adapted to undoped STO by replacing the iron ionization reaction by an ionization of a general impurity (e.g. a Sr vacancy) with an activation energy of 0.7 eV (see Table 1). For further details on the defect chemistry of STO refer to S.3.

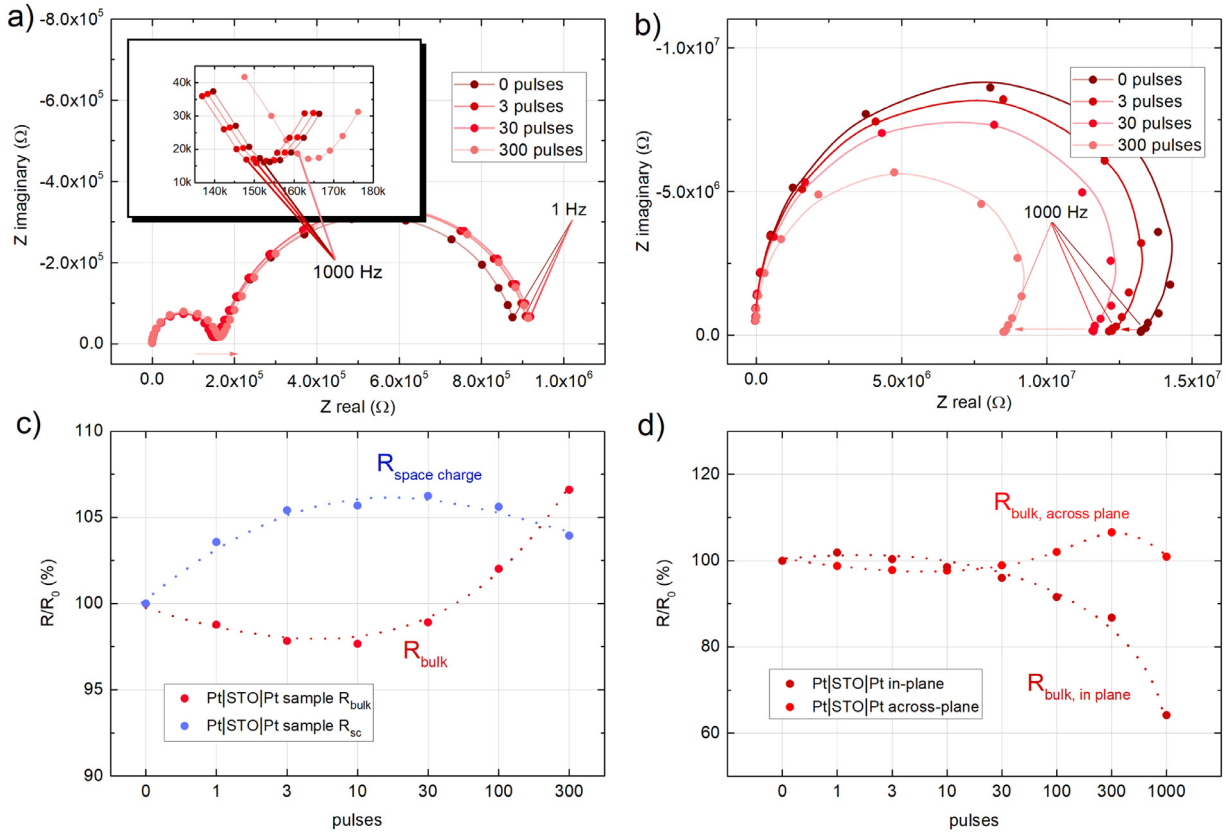

Fig. 8. Impedance spectra during PLD without cover measured at 300 °C across-plane (a) and in-plane (b). The evolution of resistances relative to their starting value is shown in c) for across plane measurements and in d) for in-plane measurements compared to across-plane measurements. Dotted lines in c) and d) are a guide for the eye.

Table 1
Mass action constants and mobility data used for calculations.

reaction	mass action constant
$V_o^{\cdot\cdot} + \frac{1}{2}O_2 \rightleftharpoons O_o^x + 2h^{\cdot}$	$4.74 \cdot 10^8$ $Pa^{-1/2}$ cm^{-3}
$A'' + h^{\cdot} \rightleftharpoons A'$	$7.04 \cdot 10^{14}$ cm^{-3}
$nil \rightleftharpoons e' + h^{\cdot}$	$7.79 \cdot 10^{16}$ cm^{-6}
species	**mobility**
$V_O^{\cdot\cdot}$	$4.78 \cdot 10^{-7}$ cm^2 V^{-1} s^{-1}
$h^{\cdot}$	0.27 cm^2 V^{-1} s^{-1}

According to this visualization, the hole conductivity increase during UV illumination from σ_0 to σ_{UV} corresponds to a change in oxygen partial pressure of about six orders of magnitude from 0.06 mbar to 60 bar, which is a strong driving force for stoichiometry changes in near-surface regions.

The extrapolation to higher temperatures, more relevant for actual deposition processes is difficult, as the surface exchange is significantly faster than at 300 °C and diffusion processes happen much faster. This is also the reason why this effect is best observed at low temperatures and 300 °C is a reasonable choice for our experiments.

We conclude that the effects of UV illumination during PLD on the substrate are clearly visible even without any direct film deposition and can alter the substrate stoichiometry significantly in near-surface regions and thus potentially also affect the growing thin film, either directly by altering its surface exchange kinetics or by a stoichiometry change induced strain.

3.3. Substrate alteration during deposition

Since during real PLD processes a wide variety of materials can be deposited on a substrate the second aim of this study was to compare the pure UV illumination effects to the impact of an actual deposition on the substrate. For this purpose the quartz cover was removed and an STO thin film was deposited onto the single crystal substrate. The same measurements were performed as during covered experiments. The results of these measurements are shown in Fig. 8.

Like during quartz covered illumination measurements, the across-plane bulk resistance of the single crystal initially decreases when material is deposited onto it. However, after more than ten pulses the value increases and rises above the initial resistance during further deposition. Also the data scattering between samples is larger than for measurements with a quartz cover. For in-plane measurements we observe again a resistance drop, however, significantly smaller than before. The combination of these results indicates that actual deposition induces changes of the substrate apart from illumination effects, which are still present. These seem to originate from processes competing with the illumination, e.g. from possible oxygen deficient deposition [11–13], thus fundamentally changing the evolution of the bulk resistance with an increasing number of pulses. Especially the strong scatter and the difference between in-plane and across-plane measurements suggest that this newly observed effect is surface related. Application of the same assumptions as before with regard to a layered sample, adding the freshly deposited film as a third layer, leads to two possible outcomes. Either the thin film is significantly less conducting and the formerly well conducting layer remains well conducting, or vice versa. However, the experimental setup renders the first option impossible, since across-plane currents should not be affected

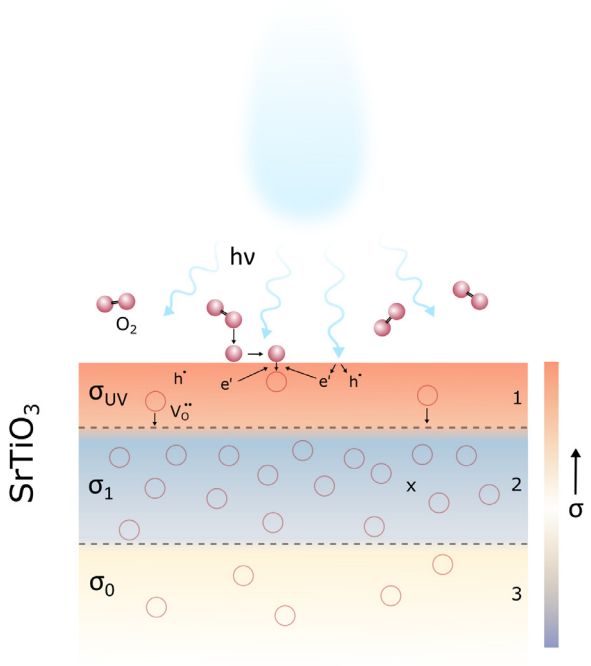

Fig. 9. Schematic of the accelerated oxygen incorporation process under UV illumination during actual deposition and the resulting layer structure.

by a thin film deposited on top. Furthermore, analysis of the calculated peak frequencies of the accompanying impedance features reveal that the bulk-assigned impedance feature would split in the first case. Hence, only the second option is viable for further discussion.

We assume that either the freshly deposited material itself or the UV illumination of this new thin film introduces a new process competing with purely substrate-related processes. Several studies have shown that PLD conditions have a substantial effect on the oxygen stoichiometry and morphology of STO thin films [53]. Furthermore it is well-known that the substrate temperature also strongly influences structure and crystallinity of the thin film and can even affect the plume propagation [2,56]. It is therefore possible that the newly deposited film is significantly oxygen deficient and extracts oxygen from the single crystal below during growth. The UV illumination additionally affects both the growing film and the substrate underneath. Consequently the growing film would be filled with oxygen even more, resulting in a more conductive thin film (σ_{UV}) and in a slightly decreased conductivity in the top layer of the single crystal (σ_1) compared to its original state (σ_0). This suggested mechanism is visualized in Fig. 9 together with the resulting layer structure of the sample.

Although the mechanisms of these processes are not yet fully understood, our experiments illustrate very clearly that an actual deposition triggers manifold and complex processes in the substrate which can also affect the thin film growth. Especially with regard to the oxygen stoichiometry during oxide deposition on photoactive substrates like for example $SrTiO_3$, TiO_2 or ZnO [57–59], such processes can not be neglected as the interaction of the substrate with the UV light will have a direct influence on the growing film, either via lattice geometry or oxidation/reduction potential.

3.4. Post-Illumination Effects

A compilation of the evolution of the bulk resistance for exemplary in-plane and across-plane measurements with and without quartz cover at 300 °C is shown in Fig. 10. According to our results conductivity changes persist after illumination. Further relaxation processes seem to occur predominantly along with actual deposition processes. Measurements at 330 °C however show that relaxation processes can also occur after illumination through a quartz cover. Independent of the exact mechanisms, the long timescale and the significant changes demonstrate that a freshly deposited sample can be driven far from equilibrium when cooled too abruptly after deposition.

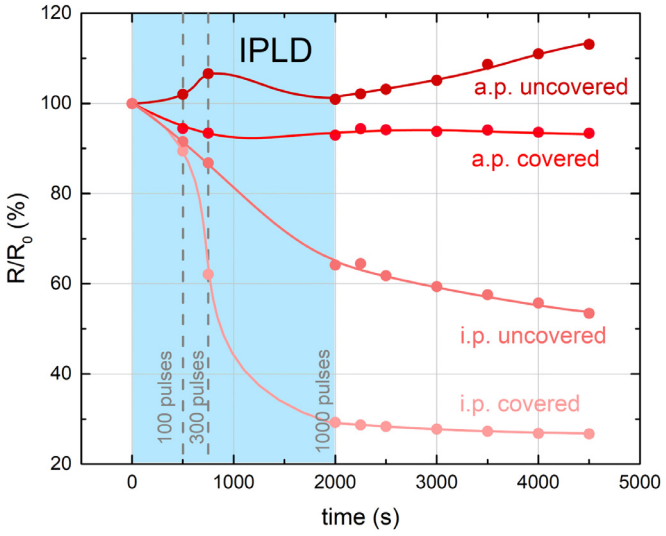

Fig. 10. Evolution of the bulk resistance for representative in-plane (i.p.) and across-plane (a.p.) measurements of covered and uncovered samples during and after illumination/deposition. Lines are a guide to the eye.

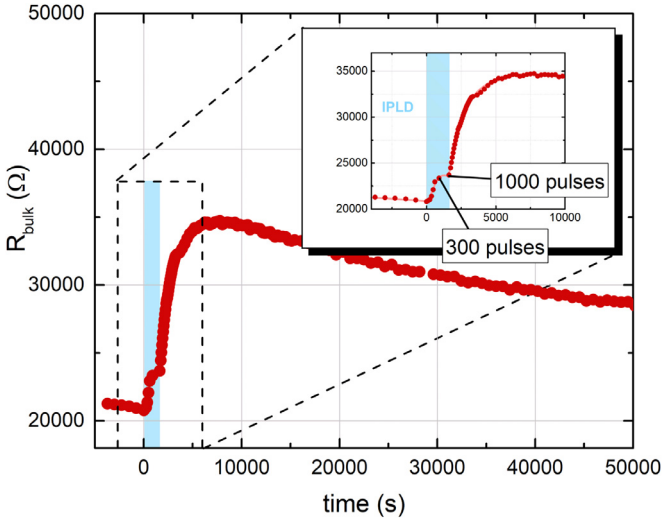

Fig. 11. Bulk resistance evolution of an STO single crystal (across-plane) before, during and after UV illumination and uncovered deposition at 330 °C. The time when laser pulses were shot is marked blue, all lines are a guide to the eye.

The aforementioned relaxation processes after uncovered deposition were further observed in across-plane geometry. These measurements showed a significant increase of the STO bulk resistance for several ten thousand seconds without quartz cover at 300 °C. To accelerate these processes a sample was measured at 330 °C (see Fig. 11). The resistance increase was again observed followed by long-lasting relaxation processes.

While the processes during illumination are partly understood, it is yet unknown, what causes the increase of the bulk resistance after illumination. Presumably, these processes originate in the

nonequilibrium conditions induced by the UV illumination. However, based on our data, no final conclusion on the mechanism is possible as of yet. It is also possible that the platinum grid or the asymmetric heating have a certain influence towards the depth dependent oxygen non-stoichiometry in STO single crystals during pulsed laser deposition.

4. Conclusions

The interaction between the plasma plume and the substrate during PLD deposition was investigated on the model system $SrTiO_3$ by means of impedance spectroscopy during pulsed laser deposition (IPLD). A significant change of the resistive properties of the substrate after deposition on a quartz cover above the sample was discovered, indicating stoichiometry changes of the substrate, causing a long-lasting increase of the STO conductivity. The results of across-plane and in-plane measurements suggest the formation of a layered system where the surface near region becomes subject to severe driving forces, corresponding to a $p(O_2)$ difference of six orders of magnitude, due to an accelerated oxygen incorporation at the sample surface under UV illumination. During real (uncovered) deposition processes, the interactions between substrate and the growing thin film become more complex and the results deviate from measurements of a covered sample. The measurements indicate a stoichiometric imbalance between substrate and growing film, resulting in a different layer structure and a different impedance response. These experiments demonstrate how the PLD process not only affects the growing thin film but also the substrate and hence, indirectly and in retrospect the thin film. Until now, only $SrTiO_3$ was investigated, but from our results we expect the observed phenomena to be important for other medium bandgap oxides as well, such as TiO_2 and ZnO.

It was discovered that the substrate undergoes long-lasting relaxation processes after the end of the deposition, possibly affecting the properties of the whole sample when cooled abruptly. We conclude that the so far mostly neglected interaction between the plasma plume and the substrate occurs in many deposition processes. It has the potential to significantly alter the properties of the substrate as well as of the growing film.

Declaration of Competing Interest

There are no conflicts of interest to declare.

Acknowledgement

Financial support by the Austrian Science Fund (FWF) project P31654-N37 is gratefully acknowledged.

Supplementary material

Supplementary material associated with this article can be found, in the online version, at doi:10.1016/j.actamat.2020.10.077.

References

[1] D.B. Chrisey, G.K. Hubler, et al., Pulsed laser deposition of thin films, Wiley New York, 1994.
[2] R. Eason, Pulsed laser deposition of thin films: applications-led growth of functional materials, John Wiley & Sons, 2007.
[3] M.N. Ashfold, F. Claeyssens, G.M. Fuge, S.J. Henley, Pulsed laser ablation and deposition of thin films, Chemical Society Reviews 33 (1) (2004) 23–31.
[4] H.M. Christen, G. Eres, Recent advances in pulsed-laser deposition of complex oxides, Journal of Physics: Condensed Matter 20 (26) (2008) 264005.
[5] Y. Zhao, Y. Jiang, Y. Fang, The influence of substrate temperature on ZnO thin films prepared by PLD technique, Journal of Crystal Growth 307 (2) (2007) 278–282.
[6] T. Ohnishi, M. Lippmaa, T. Yamamoto, S. Meguro, H. Koinuma, Improved stoichiometry and misfit control in perovskite thin film formation at a critical fluence by pulsed laser deposition, Applied Physics Letters 87 (24) (2005) 241919.
[7] M. Tyunina, S. Leppävuori, Effects of laser fluence, size, and shape of the laser focal spot in pulsed laser deposition using a multielemental target, Journal of Applied Physics 87 (11) (2000) 8132–8142.
[8] T. Yamaki, T. Sumita, S. Yamamoto, A. Miyashita, Preparation of epitaxial TiO^2 films by pld for photocatalyst applications, Journal of crystal growth 237 (2002) 574–579.
[9] T. Chen, X.M. Li, S. Zhang, H.R. Zeng, Oxygen-pressure dependence of the crystallinity of MgO films grown on Si (100) by PLD, Journal of crystal growth 270 (3–4) (2004) 553–559.
[10] F. Hensling, D. Keeble, J. Zhu, S. Brose, C. Xu, F. Gunkel, S. Danylyuk, S. Nonnenmann, W. Egger, R. Dittmann, UV radiation enhanced oxygen vacancy formation caused by the PLD plasma plume, Scientific reports 8 (1) (2018) 1–7.
[11] M.L. Scullin, J. Ravichandran, C. Yu, M. Huijben, J. Seidel, A. Majumdar, R. Ramesh, Pulsed laser deposition-induced reduction of $SrTiO_3$ crystals, Acta materialia 58 (2) (2010) 457–463.
[12] C. Schneider, M. Esposito, I. Marozau, K. Conder, M. Doebeli, Y. Hu, M. Mallepell, A. Wokaun, T. Lippert, The origin of oxygen in oxide thin films: Role of the substrate, Applied Physics Letters 97 (19) (2010) 192107.
[13] A.B. Posadas, K.J. Kormondy, W. Guo, P. Ponath, J. Geler-Kremer, T. Hadamek, A.A. Demkov, Scavenging of oxygen from $SrTiO_3$ during oxide thin film deposition and the formation of interfacial 2DEGs, Journal of Applied Physics 121 (10) (2017) 105302.
[14] R. Merkle, R.A. De Souza, J. Maier, Optically tuning the rate of stoichiometry changes: Surface-controlled oxygen incorporation into oxides under UV irradiation, Angewandte Chemie International Edition 40 (11) (2001) 2126–2129.
[15] G. Walch, B. Rotter, G.C. Brunauer, E. Esmaeili, A.K. Opitz, M. Kubicek, J. Summhammer, K. Ponweiser, J. Fleig, A solid oxide photoelectrochemical cell with UV light-driven oxygen storage in mixed conducting electrodes, Journal of Materials Chemistry A 5 (4) (2017) 1637–1649.
[16] A. Viernstein, M. Kubicek, M. Morgenbesser, G. Walch, G.C. Brunauer, J. Fleig, High-temperature photochromism of Fe-doped $SrTiO_3$ caused by UV-induced bulk stoichiometry changes, Advanced Functional Materials 29 (23) (2019) 1900196.
[17] G.C. Brunauer, B. Rotter, G. Walch, E. Esmaeili, A.K. Opitz, K. Ponweiser, J. Summhammer, J. Fleig, UV-light-driven oxygen pumping in a high-temperature solid oxide photoelectrochemical cell, Advanced Functional Materials 26 (1) (2016) 120–128.
[18] G.M. Rupp, A.K. Opitz, A. Nenning, A. Limbeck, J. Fleig, Real-time impedance monitoring of oxygen reduction during surface modification of thin film cathodes, Nature materials 16 (6) (2017) 640–645.
[19] G.M. Rupp, M. Kubicek, A.K. Opitz, J. Fleig, In situ impedance analysis of oxygen exchange on growing La0. 6Sr0. 4CoO3- δ thin films, ACS applied energy materials 1 (9) (2018) 4522–4535.
[20] C. Ahamer, A. Opitz, G. Rupp, J. Fleig, Revisiting the temperature dependent ionic conductivity of yttria stabilized zirconia (YSZ), Journal of The Electrochemical Society 164 (7) (2017) F790–F803.
[21] M.E. Orazem, B. Tribollet, Electrochemical impedance spectroscopy, John Wiley & Sons, 2017.
[22] R. Shukla, S. Patwe, S. Deshpande, S. Achary, P. Krishna, A. Shinde, J. Gopalakrishnan, A. Tyagi, Structural manipulation and tailoring of dielectric properties in $SrTi_{1-x}Fe_xTa_xO_3$ perovskites: Design of new lead free relaxors, Scientific reports 6 (1) (2016) 1–11.
[23] C. Wang, C. Lei, G. Wang, X. Sun, T. Li, S. Huang, H. Wang, Y. Li, Oxygen-vacancy-related dielectric relaxations in $SrTiO_3$ at high temperatures, Journal of Applied Physics 113 (9) (2013) 094103.
[24] R.A. De Souza, J. Fleig, J. Maier, O. Kienzle, Z. Zhang, W. Sigle, M. Rühle, Electrical and structural characterization of a low-angle tilt grain boundary in iron-doped strontium titanate, Journal of the American Ceramic Society 86 (6) (2003) 922–928.
[25] B. Sharma, Metal-semiconductor Schottky barrier junctions and their applications, Springer Science & Business Media, 2013.
[26] J. Hölzl, F.K. Schulte, H. Wagner, Solid surface physics, 85, Springer, 2006.
[27] Y.-W. Chung, W. Weissbard, Surface spectroscopy studies of the $SrTiO_3$ (100) surface and the platinum-$SrTiO_3$ (100) interface, Physical Review B 20 (8) (1979) 3456.
[28] P.C. Bowes, J.N. Baker, J.S. Harris, B.D. Behrhorst, D.L. Irving, Influence of impurities on the high temperature conductivity of $SrTiO_3$, Applied Physics Letters 112 (2) (2018) 022902.
[29] W. Rice, P. Ambwani, M. Bombeck, J. Thompson, G. Haugstad, C. Leighton, S. Crooker, Persistent optically induced magnetism in oxygen-deficient strontium titanate, Nature materials 13 (5) (2014) 481–487.
[30] J. Fleig, J. Jamnik, J. Maier, J. Ludvig, Inductive loops in impedance spectroscopy caused by electrical shielding, Journal of the Electrochemical Society 143 (11) (1996) 3636.
[31] J.-S. Lee, J. Fleig, J. Maier, D.-Y. Kim, T.-J. Chung, Local conductivity of nitrogen-graded zirconia, Journal of the American Ceramic Society 88 (11) (2005) 3067–3074.
[32] A.A. Voevodin, D.V. Shtansky, E.A. Levashov, J.J. Moore, Nanostructured thin films and nanodispersion strengthened coatings, 155, Springer Science & Business Media, 2006.
[33] T. Mieno, Plasma Science and Technology: Progress in Physical States and Chemical Reactions, BoD–Books on Demand, 2016.
[34] N. Huber, J. Gruber, N. Arnold, J. Heitz, D. Bäuerle, Time-resolved photography of the plasma-plume and ejected particles in laser ablation of polytetrafluoroethylene, EPL (Europhysics Letters) 51 (6) (2000) 674.

[35] T. Feng, Anomalous photoelectronic processes in srtio$_3$, Physical Review B 25 (2) (1982) 627.
[36] Y. Sihvonen, Photoluminescence, photocurrent, and phase-transition correlations in $SrTiO_3$, Journal of Applied Physics 38 (11) (1967) 4431–4435.
[37] P. Saadatkia, P. Stepanov, F. Selim, Photoconductivity of bulk $SrTiO_3$ single crystals at room temperature, Materials Research Express 5 (1) (2018) 016202.
[38] T. Baiatu, R. Waser, K.-H. Härdtl, DC electrical degradation of perovskite-type titanates: III, a model of the mechanism, Journal of the American Ceramic Society 73 (6) (1990) 1663–1673.
[39] S. Rodewald, N. Sakai, K. Yamaji, H. Yokokawa, J. Fleig, J. Maier, The effect of the oxygen exchange at electrodes on the high-voltage electrocoloration of Fe–doped $SrTiO_3$ single crystals: A combined sims and microelectrode impedance study, Journal of electroceramics 7 (2) (2001) 95–105.
[40] R. Waser, T. Baiatu, K.-H. Härdtl, DC electrical degradation of perovskite-type titanates: II, single crystals, Journal of the American Ceramic Society 73 (6) (1990) 1654–1662.
[41] R. Moos, K.H. Hardtl, Defect chemistry of donor-doped and undoped strontium titanate ceramics between 1000°C and 1400°C, Journal of the American Ceramic Society 80 (10) (1997) 2549–2562.
[42] W. Jung, H.L. Tuller, A new model describing solid oxide fuel cell cathode kinetics: Model thin film $SrTi_{1-x}Fe_xO_{3-\delta}$ mixed conducting oxides-a case study, Advanced Energy Materials 1 (6) (2011) 1184–1191.
[43] R.A. De Souza, V. Metlenko, D. Park, T.E. Weirich, Behavior of oxygen vacancies in single-crystal $SrTiO_3$: Equilibrium distribution and diffusion kinetics, Physical Review B 85 (17) (2012) 174109.
[44] R. Merkle, J. Maier, Oxygen incorporation into Fe-doped $SrTiO_3$: Mechanistic interpretation of the surface reaction, Physical Chemistry Chemical Physics 4 (17) (2002) 4140–4148.
[45] P. Pasierb, S. Komornicki, M. Rekas, Comparison of the chemical diffusion of undoped and Nb-doped $SrTiO_3$, Journal of Physics and Chemistry of Solids 60 (11) (1999) 1835–1844.
[46] D. Schwarz, H. Anderson, Determination of oxygen chemical diffusion coefficients in single crystal $SrTiO_3$ by capacitance manometry, Journal of The Electrochemical Society 122 (5) (1975) 707.
[47] J. Claus, M. Leonhardt, J. Maier, Tracer diffusion and chemical diffusion of oxygen in acceptor doped $SrTiO_3$, Journal of Physics and Chemistry of Solids 61 (8) (2000) 1199–1207.
[48] A. Müller, K. Härdtl, Ambipolar diffusion phenomena in $BaTiO_3$ and $SrTiO_3$, Applied Physics A 49 (1) (1989) 75–82.
[49] R. De Souza, Oxygen diffusion in $SrTiO_3$ and related perovskite oxides, Advanced Functional Materials 25 (40) (2015) 6326–6342.
[50] A. Paladino, L. Rubin, J. Waugh, Oxygen ion diffusion in single crystal $SrTiO_3$, Journal of Physics and Chemistry of Solids 26 (2) (1965) 391–397.
[51] P.W. Atkins, J. De Paula, J. Keeler, Atkins' physical chemistry, Oxford university press, 2018.
[52] I. Denk, W. Münch, J. Maier, Partial conductivities in $SrTiO_3$: bulk polarization experiments, oxygen concentration cell measurements, and defect-chemical modeling, Journal of the American Ceramic Society 78 (12) (1995) 3265–3272.
[53] H.N. Lee, S.S.A. Seo, W.S. Choi, C.M. Rouleau, Growth control of oxygen stoichiometry in homoepitaxial $SrTiO_3$ films by pulsed laser epitaxy in high vacuum, Scientific reports 6 (2016) 19941.
[54] R. Perez-Casero, J. Perriere, A. Gutierrez-Llorente, D. Defourneau, E. Millon, W. Seiler, L. Soriano, Thin films of oxygen-deficient perovskite phases by pulsed-laser ablation of strontium titanate, Physical Review B 75 (16) (2007) 165317.
[55] J. Padilla, E. Xuriguera, L. Rodríguez, A. Vannozzi, M. Segarra, G. Celentano, M. Varela, Epitaxial growth of $SrTiO_3$ films on cube-textured Cu-clad substrates by PLD at low temperature under reducing atmosphere, Nanoscale research letters 12 (1) (2017) 226.
[56] A. Sambri, S. Amoruso, X. Wang, M. Radovic, F. Miletto Granozio, R. Bruzzese, Substrate heating influence on plume propagation during pulsed laser deposition of complex oxides, Applied Physics Letters 91 (15) (2007) 151501.
[57] B. Claflin, D.C. Look, S.-J. Park, G. Cantwell, Persistent n-type photoconductivity in p-type ZnO, Journal of Crystal Growth 287 (1) (2006) 16–22.
[58] K. Hashimoto, H. Irie, A. Fujishima, TiO_2 photocatalysis: a historical overview and future prospects, Japanese journal of applied physics 44 (12R) (2005) 8269.
[59] Y. Takahashi, M. Kanamori, A. Kondoh, H. Minoura, Y. Ohya, Photoconductivity of ultrathin zinc oxide films, Japanese Journal of Applied Physics 33 (12R) (1994) 6611.